

Atmospheric Measurement Techniques Discussions is the access reviewed discussion forum of *Atmospheric Measurement Techniques*

**Reviewing
ground-based FTIR
water vapour
analysis**

M. Schneider and F. Hase

Reviewing the development of a ground-based FTIR water vapour profile analysis

M. Schneider and F. Hase

IMK-ASF, Forschungszentrum und Universität Karlsruhe, Karlsruhe, Germany

Received: 22 April 2009 – Accepted: 29 April 2009 – Published: 30 April 2009

Correspondence to: M. Schneider (matthias.schneider@imk.fzk.de)

Published by Copernicus Publications on behalf of the European Geosciences Union.

Title Page

Abstract

Introduction

Conclusions

References

Tables

Figures

⏪

⏩

◀

▶

Back

Close

Full Screen / Esc

Printer-friendly Version

Interactive Discussion

Abstract

Analytic algorithms effectively applied for ground-based infrared remote sensing of many different atmospheric trace gases can be rather ineffective for the remote sensing of tropospheric water vapour profiles. Reasons are the large vertical gradient and variability of water vapour as well as its large concentrations. We review the most important features of analysis and radiative transfer modeling required for monitoring tropospheric water vapour profiles by ground-based FTIR experiments. These are: a fit of a variety of different water vapour lines with different strength, a logarithmic scale inversion, a speed dependent Voigt line shape model, and a joint temperature profile inversion. Furthermore, the introduction of an interspecies constraint allows for a monitoring of HDO/H₂O ratio profiles.

1 Introduction

Water vapour is the most important greenhouse gas and thus, continuous observations of tropospheric water vapour amounts are essential for climate change research. The radiative forcing of water vapour depends strongly on the altitude. In the middle and upper troposphere it is much more effective as greenhouse gas than in the lower troposphere (e.g. Spencer and Braswell, 1997; Held and Soden, 2000). Consequently, long-term observations of middle/upper tropospheric water vapour amounts are of particular interest. Traditionally operational radiosondes measure upper-air water vapour. However, the radiosonde dataset is of limited consistency since a variety of different sensors has been applied during the last decades. It is difficult to use this data for trend analyses.

Ground-based high quality remote sensing experiments have the potential to observe upper-air trace gases in a continuous and consistent manner. The ground-based FTIR (Fourier Transform Infrared) experiments of NDACC (Network for Detection of Atmospheric Composition Change, Kurylo, 2000) measure high quality solar absorption

Reviewing ground-based FTIR water vapour analysis

M. Schneider and F. Hase

Title Page

Abstract

Introduction

Conclusions

References

Tables

Figures

⏪

⏩

◀

▶

Back

Close

Full Screen / Esc

Printer-friendly Version

Interactive Discussion

Reviewing ground-based FTIR water vapour analysis

M. Schneider and F. Hase

Title Page

Abstract

Introduction

Conclusions

References

Tables

Figures

⏪

⏩

◀

▶

Back

Close

Full Screen / Esc

Printer-friendly Version

Interactive Discussion



spectra since many years. These measurements disclose plenty of information about the distribution of many different atmospheric trace gases. Over the last decades the NDACC FTIR experiments were essential for studying stratospheric ozone chemistry by providing a long-term dataset of different ozone relevant trace gases (e.g. Rinsland et al., 2003; Vigouroux et al., 2008). During the last years the NDACC-FTIR community has increased its efforts of monitoring the tropospheric distribution of greenhouse gases, including water vapour.

Inversion methods for atmospheric remote sensing are treated extensively in the textbook of Rodgers (2000). However, the inversion of atmospheric water vapour amounts from ground-based FTIR spectra is no typical atmospheric inversion problem. The large vertical gradient and variability is the main reason why standard retrieval methods are not suited. First vertical profiles of water vapour measured by ground-based FTIR experiments were reported by a group of the Institute for Meteorology and Climate Research, Karlsruhe, Germany (in German letters: IMK-ASF; Hase et al., 2004). During the last years, the IMK-ASF water vapour analysis has been continuously developed and improved (Schneider et al., 2006a,b; Schneider and Hase, 2009). These efforts made it possible to monitor tropospheric H₂O profiles (including upper tropospheric amounts) and HDO/H₂O ratio profiles by ground-based FTIR experiments.

This paper reviews the aspects of an effective ground-based FTIR water vapour analysis. Section 2 briefly describes the principles of a ground-based FTIR analysis and in Sect. 3 we discuss the methods developed at IMK-ASF to overcome the difficulties of water vapour analysis. Section 4 lists these developments in the order of their importance.

2 General setup of a ground-based FTIR analysis

The basic equation for analysing solar absorption spectra is Lambert Beer's law:

$$I(\lambda) = I_{\text{sun}}(\lambda) \exp\left(-\int_{\text{TOA}}^{\text{Obs.}} \sigma_x(\lambda, s(T, p)) x(s) ds\right) \quad (1)$$

Reviewing ground-based FTIR water vapour analysis

M. Schneider and F. Hase

Title Page

Abstract

Introduction

Conclusions

References

Tables

Figures

◀

▶

◀

▶

Back

Close

Full Screen / Esc

Printer-friendly Version

Interactive Discussion



Here $I(\lambda)$ is the measured intensity at wavelength λ , I_{sun} the solar intensity, $\sigma_x(\lambda, s)$ is the absorption cross section and $x(s)$ the concentration of an absorber x at location s . The integration is performed along the path of the direct sunlight (between the Observer (Obs.) and the Top of the atmosphere (TOA)). The spectra are simulated
 5 by a precise line-by-line radiative transfer model applying the parameters of spectroscopic databases (e.g. HITRAN, Rothman et al., 2005). Within NDACC mid-infrared ground-based FTIR spectra are typically measured with a resolution of 0.005 cm^{-1} . Equation (1) neglects atmospheric emission. However, at low frequencies (below approximately 1000 cm^{-1}) or when analysing lunar absorption spectra (Palm et al., 2008)
 10 it should be considered, by adding an atmospheric emission correction term.

For the purpose of numerical handling the atmospheric state $x(s)$ and the simulated spectrum $I(\lambda)$ are discretised in form of a state vector \mathbf{x} and a measurement vector \mathbf{y} . The measurement and state vector are related by a vector valued function F which simulates the atmospheric radiative transfer and the characteristics of the measurement
 15 system (spectral resolution, instrumental line shape, etc.):

$$\mathbf{y} = F(\mathbf{x}) \quad (2)$$

The derivatives $\partial \mathbf{y} / \partial \mathbf{x}$ determine the changes in the spectral fluxes \mathbf{y} for changes in the vertical distribution of the absorber \mathbf{x} . These derivatives are collected in a Jacobian matrix \mathbf{K} :

$$\partial \mathbf{y} = \mathbf{K} \partial \mathbf{x} \quad (3)$$

Direct inversion of Eq. (3) would allow an iterative calculation of the sought variables \mathbf{x} . However, generally the problem is under-determined, i.e. the columns of \mathbf{K} are not linearly independent and there are many solutions that are in acceptable agreement with the measurement. An optimal estimation (OE) approach removes this ambiguity.
 25 It combines the measurement information with the a priori assumption about the atmospheric state and selects the most probable state for the given measurement. The solution is the maximum value of a conditional probability density function (pdf), which

Reviewing ground-based FTIR water vapour analysis

M. Schneider and F. Hase

Title Page

Abstract

Introduction

Conclusions

References

Tables

Figures

◀

▶

◀

▶

Back

Close

Full Screen / Esc

Printer-friendly Version

Interactive Discussion



is the product of two pdfs: a first, describing the statistics of the differences between simulated and measured spectra (measurement noise covariance \mathbf{S}_e), and a second, describing the a priori knowledge of the atmospheric state (mean state \mathbf{x}_a and covariance \mathbf{S}_a). The maximum value of the conditional pdf is reached at the minimum of its negative logarithm. Therefore, we have to minimise:

$$[\mathbf{y} - F(\mathbf{x})]^T \mathbf{S}_e^{-1} [\mathbf{y} - F(\mathbf{x})] + [\mathbf{x} - \mathbf{x}_a]^T \mathbf{S}_a^{-1} [\mathbf{x} - \mathbf{x}_a] \quad (4)$$

Due to the non-linear behavior of the Lambert Beer law (Eq. 1), the cost function (Eq. 4) is minimised iteratively by a Gauss-Newton method. The solution for the $(i+1)$ th iteration is (Rodgers, 2000):

$$\mathbf{x}_{i+1} = \mathbf{x}_a + \mathbf{S}_a \mathbf{K}_i^T (\mathbf{K}_i \mathbf{S}_a \mathbf{K}_i^T + \mathbf{S}_e)^{-1} [\mathbf{y} - F(\mathbf{x}_i) + \mathbf{K}_i (\mathbf{x}_i - \mathbf{x}_a)] \quad (5)$$

An important component of the retrieved solution is the averaging kernel matrix \mathbf{A} :

$$\mathbf{A} = (\mathbf{K}^T \mathbf{S}_e^{-1} \mathbf{K} + \mathbf{S}_a^{-1})^{-1} \mathbf{K}^T \mathbf{S}_e^{-1} \mathbf{K} \quad (6)$$

The trace of \mathbf{A} quantifies the amount of information introduced by the measurement. It can be interpreted in terms of degrees of freedom of the measurement (DOF). The averaging kernel matrix \mathbf{A} describes the smoothing of the atmospheric state (i.e. the vertical distribution of the absorber) by the FTIR measurement process. It relates the real variability ($\mathbf{x} - \mathbf{x}_a$) to the measured variability ($\hat{\mathbf{x}} - \mathbf{x}_a$):

$$(\hat{\mathbf{x}} - \mathbf{x}_a) = \hat{\mathbf{A}} (\mathbf{x} - \mathbf{x}_a) \quad (7)$$

3 Particularities of a water vapour analysis

In recent years at IMK-ASF we continuously extended the standard FTIR analysis by several innovative features, which allow an effective analysis of water vapour profiles.

**Reviewing
ground-based FTIR
water vapour
analysis**M. Schneider and F. Hase

[Title Page](#)[Abstract](#)[Introduction](#)[Conclusions](#)[References](#)[Tables](#)[Figures](#)[⏪](#)[⏩](#)[◀](#)[▶](#)[Back](#)[Close](#)[Full Screen / Esc](#)[Printer-friendly Version](#)[Interactive Discussion](#)

The features are as follows: first, the application of a variety of weak and strong water vapour lines, which makes the retrievals very sensitive to both extremely low and high water vapour amounts. Second, a logarithmic scale inversion. Only this assures a proper constraint of tropospheric water vapour amounts (Schneider et al., 2006a; Worden et al., 2006a; Deeter et al., 2007). Third, a constraint of H₂O profiles against HDO profiles. This allows for an inversion of tropospheric HDO/H₂O ratio profiles (Schneider et al., 2006b; Worden et al., 2006a), which are useful for investigating the transport pathways of tropospheric water vapour. Fourth, the application of a non-Voigt line shape model for a proper simulation of the water vapour lines (Boone et al., 2007; Schneider and Hase, 2009). Fifth, the consideration of atmospheric emissions for a proper simulation of radiances at low frequencies. And sixth, a simultaneous temperature profile inversion. This reduces two important error sources of ground-based FTIR measurements, which are uncertainties in the assumed temperature profiles and uncertainties in the temperature dependence of the applied spectroscopic parameters (Schneider et al., 2006a, 2008; Schneider and Hase, 2008).

In the following Subsections we document the improvements achieved by these innovations, therefore we document the performance of 6 different FTIR analysis setups:

- lin: inversion on a linear scale.
- log: inversion on a logarithmic scale.
- log, isc: log-scale and H₂O, H₂¹⁸O, and HDO inter-species constraint.
- log, isc, nV: log-scale, inter-species constraint, and non-Voigt line shape model.
- log, isc, nV, ae: log-scale, inter-species constraint, non-Voigt line shape, and correction for atmospheric emission.
- log, isc, nV, ae, T: log-scale, inter-species constraint, non-Voigt line shape, atmospheric emission, and simultaneous temperature profile inversion.

The documentation consists of a theoretical part, by analysing the DOF values achieved by the different analysis setups, and of an empirical part, by comparing the

Reviewing ground-based FTIR water vapour analysis

M. Schneider and F. Hase

Title Page

Abstract

Introduction

Conclusions

References

Tables

Figures

◀

▶

◀

▶

Back

Close

Full Screen / Esc

Printer-friendly Version

Interactive Discussion



FTIR profiles to radiosonde measurements. We do this taking measurements performed at the Izaña Atmospheric Research Centre (in Spanish letters: CIAI) as an example, since at CIAI water vapour radiosonde measurements (Vaisala RS92) are performed twice daily. The quality documentation is based on a representative set of measurements, which cover a large variety of different atmospheric water vapour states, taken on 93 different days between June 2005 and February 2007.

Concerning the empirical validation we have to consider that an FTIR measurement takes less than 10 min, but a radiosonde needs about 1 h to measure a profile from the ground to 15 km. As temporal coincidence criterion we require that the RS92 radiosonde is located at 7.5 km within 2 h of the FTIR measurement. For the comparison we adjust the vertically highly-resolved Vaisala RS92 profile (x_{RS92}) to the modest vertical resolution of the FTIR profiles by a convolution with the FTIR averaging kernels $\hat{\mathbf{A}}$. The columns of a typical averaging kernel matrix $\hat{\mathbf{A}}$ are shown in Fig. 1. According to Eq. (7) it is:

$$\hat{x}_{\text{RS92}} = \hat{\mathbf{A}}(x_{\text{RS92}} - x_a) + x_a \quad (8)$$

The result is an RS92 profile (\hat{x}_{RS92}) with the same vertical resolution as the FTIR profile. In addition we apply the temperature and radiation correction for the RS92 sensor as suggested by Vömel et al. (2007).

3.1 Simultaneous fit of weak and strong lines

Atmospheric water vapour is highly variable, e.g. the total precipitable water vapour (PWV) amount varies almost over 2 orders of magnitude. This requires the application of water vapour lines with different characteristics. Strong lines are necessary to be sensitive in the case of low water vapour amounts. However, these lines are saturated at large water vapour amounts. Therefore, weak lines have to be included into the spectral microwindows. Figure 2 plots the degrees of freedom of the measurement (DOF) versus the total water vapour content along the line of sight (slant PWV). If we apply a spectral microwindow with a weak water vapour line, the DOF value is around

**Reviewing
ground-based FTIR
water vapour
analysis**M. Schneider and F. Hase

[Title Page](#)[Abstract](#)[Introduction](#)[Conclusions](#)[References](#)[Tables](#)[Figures](#)[⏪](#)[⏩](#)[◀](#)[▶](#)[Back](#)[Close](#)[Full Screen / Esc](#)[Printer-friendly Version](#)[Interactive Discussion](#)

2.1, but tends to lower values for slant PWVs below 3 mm (left panel). The central panel shows the situation when applying a strong line. For slant PWVs below 8 mm we obtain larger DOF values if compared to the “weak line retrieval”. However, this strong line is saturated for slant PWVs above 10 mm. For large slant PWVs the DOF values are rapidly decreasing. The right panel depicts the DOFs for a retrieval which applies both the weak and the strong line. Then we achieve satisfactory results in the case of low and large slant PWVs.

Our IMK-ASF water vapour analysis algorithm applies 49 water vapour lines of different strength (37 H₂O, 3 H₂¹⁸O, and 9 HDO lines) between 790 and 1330 cm⁻¹. The corresponding spectral microwindows are shown in Fig. 3. With this setup we achieve DOF values between 2.2 and 3.0 (see Fig. 5).

3.2 Logarithmic scale inversion

Equation (4) assumes Gaussian statistics for the measurement noise and the a priori covariance. While Gaussian statistics is a valid assumption for the measurement noise it is not necessarily valid for the distribution of the absorber. Highly variable absorbers like water vapour are necessarily not normally distributed. However, by performing the inversion on a linear scale we implicitly assume a normal distribution. Under these circumstances minimising the cost function (Eq. 4) does not yield a statistically optimal solution. If the inversion is performed on a linear scale the FTIR profiles significantly disagree with the RS92 profiles, which is documented by the left panels of Fig. 4: the top panel depicts the differences of all 93 FTIR/RS92 coincidences and the bottom panel its statistics (mean and standard deviation of the difference). Frequently the FTIR analysis produces physically impossible negative volume mixing ratios, i.e. $\frac{\text{FTIR}}{\text{RS92}} - 1 < -100\%$.

Like most highly variable atmospheric constituents, water vapour is quite well log-normally distributed and so we can improve the optimal estimation formalism of Eqs. (4) and (5) by transforming the absorber’s amounts to a logarithmic scale: if x is log-normally distributed $\ln(x)$ is normally distributed and Eqs. (4) and (5) remain valid. The

Reviewing ground-based FTIR water vapour analysis

M. Schneider and F. Hase

Title Page

Abstract

Introduction

Conclusions

References

Tables

Figures

⏪

⏩

◀

▶

Back

Close

Full Screen / Esc

Printer-friendly Version

Interactive Discussion



second panels from the left show the comparison of the RS92 and FTIR profiles when the inversion is performed on a logarithmic scale. The log-scale inversion significantly reduces the scatter between the RS92 and the FTIR data, in particular below 7 km. Figure 5 depicts the degrees of freedom of the measurement (DOF) versus the PWV. The left panel shows the situation for a linear scale inversion and the second panel from the left for a logarithmic scale inversion. These plots give further insight in the deficiencies of a linear scale water vapour inversion. We observe that for a linear scale inversion the DOF decreases continuously with increasing PWV. This strong dependence is due to an inadequate constraint caused by applying a wrong a prior statistics. At low PWVs the constraint is too weak and at large PWVs it is too strong. The DOF values in case of a logarithmic scale inversion show a much weaker dependence on PWV. Its DOF values only decrease when a increasing number of lines becomes saturated (for slant PWVs above 7 mm).

Table 1 collects the scatter between the PWVs determined by the different FTIR analysis and by RS92 and Cimel sunphotometer (Holben et al., 1998) measurements. We only compare if all three experiments coincide within 1 h (88 coincidences). For these coincidences the scatter of $\frac{(RS92-Cimel)}{(RS92+Cimel)/2}$ is 19.6%. For a linear scale inversion the scatter of $\frac{(FTIR-RS92)}{(FTIR+RS92)/2}$ and $\frac{(FTIR-Cimel)}{(FTIR+Cimel)/2}$ are 14.5% and 13.5%, respectively. The root-square-sum (RSS) of these values is $\sqrt{14.5^2+13.5^2}\%=19.8\%$. For independent FTIR, RS92, and Cimel errors we can estimate the precision of the FTIR PWV data to $\sqrt{\frac{19.8^2-19.6^2}{2}}\%=2.0\%$. If we apply a log-scale inversion the scatter between the FTIR and the other experiments reduces to $\pm 14.1\%$ and $\pm 13.4\%$, respectively, and the RSS to $\sqrt{14.1^2+13.4^2}\%=19.5\%$. This value is smaller than the scatter between the RS92 and Cimel PWV data of 19.6% and means that the FTIR PWV data obtained by a log-scale inversion are extremely precise.

3.3 HDO/H₂O ratio profiles

The isotopic composition of tropospheric water vapour depends on the Ocean surface conditions where it evaporates and on its atmospheric transport pathways. Measurements of HDO/H₂O are a powerful tool for investigating atmospheric dynamics and in particular water vapour transport pathways (Worden et al., 2006b; Yoshimura et al., 2008), which in turn is important for a better understanding of global climate change (water vapour feedback effect). Infrared remote sensing offers a unique opportunity for a continuous observation of the HDO/H₂O ratio, which is typically expressed in form of a δD value. The δD value is the relative difference of the actual HDO/H₂O ratio to the standard HDO/H₂O ratio called SMOW (Standard Mean Ocean Water) in permil ($\delta D = 1000 \times \left(\frac{[\text{HDO}]/[\text{H}_2\text{O}]}{\text{SMOW}} - 1 \right)$).

Figure 6 shows δD profiles as obtained from different analysis algorithms. The left panel shows the situation for independent H₂O and HDO inversions. Then the δD values vary between -1000 and $+4000$, which is physically impossible. The reason of these large errors is the absence of an HDO/H₂O constraint. Since H₂O and HDO have different vertical resolutions their profiles are not comparable and a simple rationing produces unreasonable results. The logarithmic scale inversion allows for an optimal estimation of HDO/H₂O profiles, by constraining $\ln[\text{HDO}] - \ln[\text{H}_2\text{O}]$ (Schneider et al., 2006b; Worden et al., 2006a). This procedure produces statistically optimised HDO/H₂O profiles, which are depicted in the second panel from the left of Fig. 6. Applying the the HDO versus H₂O inter-species constraints we observe reasonable HDO/H₂O ratios, which are situated between -700 and $+50$.

The inter-species constraint also improves the agreement between RS92 and FTIR water vapour profiles, as can be observed in the third panel from the left of Fig. 4. Atmospheric HDO amounts are by more than three orders of magnitude lower than H₂O amounts. Whereas we have to fit H₂O lines corresponding to transitions between states with high quantum numbers, we can fit HDO lines which involve states with low quantum numbers. We assume that the spectroscopic knowledge of the strongest

**Reviewing
ground-based FTIR
water vapour
analysis**

M. Schneider and F. Hase

Title Page

Abstract

Introduction

Conclusions

References

Tables

Figures

⏪

⏩

◀

▶

Back

Close

Full Screen / Esc

Printer-friendly Version

Interactive Discussion

HDO lines is better than the spectroscopic knowledge of the weak H₂O transitions. The inter-species constraint partly reduces the misinterpretation of the H₂O signatures, but, due to inconsistencies between the H₂O and the HDO line parameters, it increase the residuals (difference between measured and simulated spectrum). As a consequence the DOF values are slightly reduced (see third panel from the left of Fig. 5).

3.4 Proper line shape model

Applying lines with different strength and pressure broadening coefficients theoretically increases the DOF value, but in practice there is no realistic water vapour profile that brings measured and simulated signatures of all the different lines in a reasonable agreement. In Schneider and Hase (2009) we analysed this problem in more detail and found that applying a speed dependent Voigt line shape model instead of a Voigt line shape model provides a much better agreement between the simulated and measured high-resolution spectra and at the same time improves the quality of the inverted water vapour profiles. This is in agreement with Boone et al. (2007) who recommended the application of a speed dependent Voigt line shape model when analysing the infrared spectra measured by ACE (Atmospheric Chemistry Experiment). The improved agreement between measured and simulated spectrum is documented by comparing the two panels from the bottom of Fig. 3. The first panel shows the residuals (difference between measured and simulated spectrum) when applying a Voigt line shape model and the HITRAN 2004 parameters (Rothman et al., 2005) with the water vapour update of Gordon et al. (2007). The second panel depicts the residuals for a speed dependent Voigt line shape model (Boone et al., 2007) that applies the parameters of Schneider and Hase (2009). The improvement in the quality of the inverted water vapour profile is documented in Fig. 4 when comparing the third panel from the left, where profiles are inverted by applying a Voigt line shape model and the Gordon et al. (2007) water vapour line parameters, with the fourth panel from the left, where a speed dependent Voigt line shape model and the Schneider and Hase (2009) parameters are applied.

In addition, applying a proper line shape model allows for a correct interpretation

**Reviewing
ground-based FTIR
water vapour
analysis**

M. Schneider and F. Hase

Title Page

Abstract

Introduction

Conclusions

References

Tables

Figures

⏪

⏩

◀

▶

Back

Close

Full Screen / Esc

Printer-friendly Version

Interactive Discussion



of the measured spectrum and leads to larger DOF values. This can be observed by comparing the third and the fourth panel from the left of Fig. 5.

Figure 6 demonstrates that applying a speed dependent Voigt line shape model also improves the quality of the δD profiles. They are now in reasonable agreement with the a priori expected δD profiles (third panel from the left), whereas the δD profiles produced by applying a Voigt line shape model show an unexpected maxima at about 7 km (second panel from the left).

3.5 Atmospheric emissions

Often the line-by-line models used for simulating solar absorption spectra approximate the radiances by applying Eq. (1), which disregards atmospheric emissions. Figure 7 shows the relative absorption at the line centres (i.e. baseline offset at the line centre related to the spectral intensity at the line shoulders) of two strong water vapour lines versus the slant PWVs. The black squares show the measurement. Both lines are saturated for slant PWVs above 3 mm. We observe that the baseline offset at 796 cm^{-1} is 0.4%, and at 1198 cm^{-1} it is 0.1%. We find that for frequencies below approx. 1000 cm^{-1} the baseline offset caused by atmospheric emission is larger than the measurement noise. The blue triangles depict radiances simulated according to Eq. (1), i.e. by disregarding atmospheric emission, and the red circles show the calculation which include atmospheric emissions. We observe that the baseline offset is dominated by atmospheric emission. The upward bending of 0.002–0.007% (see blue triangles), caused by numerical approximations in the radiative transfer modeling, is almost two orders of magnitude smaller and thus irrelevant.

The consideration of atmospheric emission prevents from a misinterpretation of strong water vapour signatures at low frequencies. Considering atmospheric emission slightly increases the DOF values by 0.1 and reduces the DOF 1σ variability by 0.1 (compare fourth and fifth panel from the left of Fig. 5). In addition it slightly improves the quality of the FTIR water vapour profiles (the scatter and mean difference to the RS92 profile are reduced; compare fourth and fifth panel from the left of Fig. 4). In the

**Reviewing
ground-based FTIR
water vapour
analysis**

M. Schneider and F. Hase

Title Page

Abstract

Introduction

Conclusions

References

Tables

Figures

◀

▶

◀

▶

Back

Close

Full Screen / Esc

Printer-friendly Version

Interactive Discussion



case of solar absorption spectra these effects are very small, since the intensity of the atmospheric emission is less than 0.5% of the solar intensity. However, when analysing lunar absorption spectra it is essential to consider atmospheric emission (Palm et al., 2008).

5 3.6 Joint inversion of temperature profiles

The cross sections σ_x (see Eq. 1) depend on temperature and pressure. Standard inversion algorithms apply temperature profiles from Reanalysis calculations or data measured close to the FTIR site by radiosondes. However, these data may be erroneous, first, due to errors in the radiosonde observations (Reanalysis data are also based on radiosonde measurements), and second, due to temporal and spatial mismatch between radiosonde and FTIR measurements. Schneider and Hase (2008) showed that for standard O₃ inversions these temperature uncertainties are the leading error source and they suggested to invert the temperature profile simultaneously with the trace gas profile. In the case of O₃ a joint inversion of temperature profiles significantly improves the quality of the FTIR O₃ data (Schneider and Hase, 2008; Schneider et al., 2008).

The fifth and sixth panel from the left of Fig. 4 document how a joint inversion of temperature profiles improves the quality of the FTIR water vapour profiles. If the Reanalysis or radiosonde temperatures are used, we observe a mean difference and scatter between RS92 and FTIR of (+26.1±33.5)% at 3 km, (-18.3±24.8)% at 5 km, and (-2.3±29.4)% at 9 km. For a joint inversion of the temperature profile we get (-15.3±19.7)%, and (+2.7±19.3)% at 5, and 9 km, respectively. Then the middle and upper tropospheric FTIR water vapour amounts are of very good quality, since the remaining scatter of about 20% is in agreement with the expected uncertainty of the RS92 data (Vömel et al., 2007). Surprisingly, in the lower troposphere the scatter slightly increase from ±33.5% to ±38.1%. We think that this increase is not significant given the relatively large inhomogeneity in lower tropospheric water vapour fields and the fact that the RS92 and FTIR detect different airmasses.

Reviewing ground-based FTIR water vapour analysis

M. Schneider and F. Hase

Title Page

Abstract

Introduction

Conclusions

References

Tables

Figures

⏪

⏩

◀

▶

Back

Close

Full Screen / Esc

Printer-friendly Version

Interactive Discussion

The joint temperature inversion also reduces the variability in δD values as retrieved for the lower troposphere, from 110 permil to 95 (compare third and fourth panel from the left of Fig. 6), providing for a better agreement with other lower tropospheric δD measurements (e.g. Ehhalt, 1974).

Concerning the DOF values the joint temperature inversion slightly increases the DOFs for measurements made at high slant PWVs and slightly decreases the DOFs for measurements made at low slant PWVs (see Fig. 5). The 1σ variability of the DOFs for the analysed ensemble reduces to 0.22, i.e. the profiles produced for different atmospheric conditions are well consistent.

4 Conclusions

Tropospheric water vapour is highly variable. For a precise monitoring of both very humid and very dry atmospheric states the application of many different lines with different strength and pressure broadening coefficients is essential. Furthermore, the inversion must be performed on a logarithmic scale. Only this assures a proper constraint of tropospheric water vapour amounts and a statistically optimal solution. In addition, the logarithmic scale inversion allows for an optimal estimation of HDO/H₂O ratio profiles. A linear scale inversion provides no statistically optimal solution and no possibility for an optimal estimation of HDO/H₂O ratios. Then the produced water vapour profiles are of poor quality and the HDO/H₂O ratio profiles useless.

The logarithmic scale inversion is an important progress, but for an effective ground-based FTIR water vapour inversion we need to remove the inconsistencies when simulating the spectral signatures of a large number of different lines. In particularly large is the inconsistency between the HDO lines (situated above 1220 cm⁻¹) and the H₂O lines (between 775 and 1200 cm⁻¹). The application of a speed dependent Voigt line shape model together with the parameters of Schneider and Hase (2009) removes a large part of these inconsistencies and significantly improves the quality of the FTIR profiles. Applying a large set of weak and strong water vapour signatures, performing

Reviewing ground-based FTIR water vapour analysis

M. Schneider and F. Hase

Title Page

Abstract

Introduction

Conclusions

References

Tables

Figures

⏪

⏩

◀

▶

Back

Close

Full Screen / Esc

Printer-friendly Version

Interactive Discussion

**Reviewing
ground-based FTIR
water vapour
analysis**M. Schneider and F. Hase

[Title Page](#)[Abstract](#)[Introduction](#)[Conclusions](#)[References](#)[Tables](#)[Figures](#)[⏪](#)[⏩](#)[◀](#)[▶](#)[Back](#)[Close](#)[Full Screen / Esc](#)[Printer-friendly Version](#)[Interactive Discussion](#)

the inversion on a log-scale, and using a speed dependent Voigt line shape model adequately exploits ground-based FTIR measurements. The FTIR system provides then tropospheric water vapour profiles with a precision of better than 25–30% and reasonable HDO/H₂O ratio profiles. Our analysis recipes significantly reduce the dependency of the DOFs on the atmospheric condition, i.e. they produce consistent profiles even for largely varying atmospheric water vapour contents. Our recipes also improve the precision of the total precipitable water vapour (PWV) amounts as documented by Table 1. Our FTIR analysis technique provides PWVs with a precision of better than 1%.

Considering atmospheric emission and, in particular, performing a joint temperature profile inversion further improves the quality of the FTIR profiles. Then the scatter between the RS92 and the FTIR data is reduced to 20%, which is the expected precision of the RS92 data. This means that when applying all the features of the IMK-ASF water vapour inversion algorithm as presented in Sect. 3 a ground-based FTIR system provides very precise tropospheric water vapour profiles with the vertical resolution as documented in Fig. 1.

Acknowledgements. The FTIR activities are supported by the European Commission and the Deutsche Forschungsgemeinschaft by funding via the projects SCOUT-O3 and GEOMON (contract SCOUT-O3-505390 and GEOMON-036677) and RISOTO (Geschäftszeichen SCHN 1126/1-1), respectively. We are grateful to the Goddard Space Flight Center for providing the temperature and pressure profiles of the National Centers for Environmental Prediction via the automailer system. We thank the colleagues from the Izaña Atmospheric Research Centre, in particular Mr. S. Afonso, for providing the RS92 data.

References

- Boone, C. D., Walker, K. A., and Bernath, P. F.: Speed-dependent Voigt profile for water vapor in infrared remote sensing applications, *J. Quant. Spectrosc. Ra.*, 105, 525–532, 2007. 1226, 1231
- Holben, B. N., T. F. Eck, I. Slutsker, D. Tanré, Buis, J. P., Setzer, A., Vermote, E., Reagan, J. A., Kaufman, Y. J., Nakajima, T., Lavenu, F., Jankowiak, I., and Smirnov, A.: AERONET

– A Federated Instrument Network and Data Archive for Aerosol Characterization, Remote Sens. Environ., 66, 1–16, 1998. 1229

Deeter, M. N., Edwards, D. P., and Gille, J. C.: Retrievals of carbon monoxide profiles from MOPITT observations using lognormal a priori statistics, J. Geophys. Res., 112, D11311, doi:10.1029/2006JD007999, 2007. 1226

Ehhalt, D. H.: Vertical profiles of HTO, HDO, and H₂O in the Troposphere, Rep. NCAR-TN/STR-100, Natl. Cent. for Atmos. Res., Boulder, CO, USA, 1974. 1234

Gordon, E. I., Rothman, L. S., Gamache, R. R., Jacquemart, D., Boone, C., Bernath, P. F., Shephard, M. W., Delamere, J. S., and Clough, S. A.: Current updates of the water-vapor line list in HITRAN: A new “Diet” for air-broadened half-widths, J. Quant. Spectrosc. Ra., 108, 389–402, 2007. 1231, 1242

Hase, F., Hannigan, J. W., Coffey, M. T., Goldman, A., Höpfner, M., Jones, N. B., Rinsland, C. P., and Wood, S. W.: Intercomparison of retrieval codes used for the analysis of high-resolution, ground-based FTIR measurements, J. Quant. Spectrosc. Ra., 87, 25–52, 2004. 1223

Held, I. M. and Soden, B. J.: Water Vapour Feedback and Global Warming, Annu. Rev. Energ. Env., 25, 441–475, 2000. 1222

Kurylo, M. J. and Zander, R.: The NDSC – Its status after 10 years of operation, Proceedings of XIX Quadrennial Ozone Symposium, Hokkaido University, Sapporo, Japan, 167–168, 2000. 1222

Palm, M., Melsheimer, C., Noël, S., Notholt, J., Burrows, J., and Schrems, O.: Integrated water vapor above Ny Ålesund, Spitsbergen: a multisensor intercomparison, Atmos. Chem. Phys. Discuss., 8, 21171–21199, 2008, <http://www.atmos-chem-phys-discuss.net/8/21171/2008/>. 1224, 1233

Rinsland, C. P., Mahieu, E., Zander, R., Jones, N. B., Chipperfield, M. P., Goldman, A., Anderson, J., Russell III, J. M., Demoulin, P., Notholt, J., Toon, G. C., Blavier, J.-F., Sen, B., Sussmann, R., Wood, W., Meier, A., Griffith, D. W. T., Chiou, L. S., Murcray, F. J., Stephen, T. M., Hase, F., Mikuteit, S., Schultz, A., and Blumenstock T.: Long-Term Trends of Inorganic Chlorine from Ground-Based Infrared Solar Spectra: Past Increases and Evidence for Stabilization, J. Geophys. Res., 108(D8), 4252, doi:10.1029/2002JD003001, 2003. 1223

Rodgers, C. D.: Inverse Methods for Atmospheric Sounding: Theory and Praxis, World Scientific Publishing Co., Singapore, ISBN 981-02-2740-X, 2000. 1223, 1225

Rothman, L. S., Jacquemart, D., Barbe, A., Benner, D. C., Birk, M., Brown, L. R., Carleer, M. R., Chackerian Jr., C., Chance, K. V., Coudert, L. H., Dana, V., Devi, J., Flaud, J.-M., Gamache,

Reviewing ground-based FTIR water vapour analysis

M. Schneider and F. Hase

Title Page

Abstract

Introduction

Conclusions

References

Tables

Figures

◀

▶

◀

▶

Back

Close

Full Screen / Esc

Printer-friendly Version

Interactive Discussion

**Reviewing
ground-based FTIR
water vapour
analysis**M. Schneider and F. Hase

[Title Page](#)[Abstract](#)[Introduction](#)[Conclusions](#)[References](#)[Tables](#)[Figures](#)[⏪](#)[⏩](#)[◀](#)[▶](#)[Back](#)[Close](#)[Full Screen / Esc](#)[Printer-friendly Version](#)[Interactive Discussion](#)

R. R., Goldman, A., Hartmann, J. M., Jucks, K. W., Maki, A. G., Mandin, J. Y., Massie, S. T., Orphal, J., Perrin, A., Rinsland, C. P., Smith, M. A. H., Tennyson, J., Tolchenov, R. N., Toth, R. A., Vander-Auwera, J., Varanasi, P., and Wagner, G. The HITRAN 2004 molecular spectroscopic database, *J. Quant. Spectrosc. Ra.*, 96, 139–204, 2005. 1224, 1231, 1242

5 Schneider, M., Hase, F., and Blumenstock, T.: Water vapour profiles by ground-based FTIR spectroscopy: study for an optimised retrieval and its validation, *Atmos. Chem. Phys.*, 6, 811–830, 2006a,

<http://www.atmos-chem-phys.net/6/811/2006/>. 1223, 1226

Schneider, M., Hase, F., and Blumenstock, T.: Ground-based remote sensing of HDO/H₂O ratio profiles: introduction and validation of an innovative retrieval approach, *Atmos. Chem. Phys.*, 6, 4705–4722, 2006b,

<http://www.atmos-chem-phys.net/6/4705/2006/>. 1223, 1226, 1230

Schneider, M. and Hase, F.: Technical Note: Recipe for monitoring of total ozone with a precision of around 1 DU applying mid-infrared solar absorption spectra, *Atmos. Chem. Phys.*, 8, 63–71, 2008,

<http://www.atmos-chem-phys.net/8/63/2008/>. 1226, 1233

Schneider, M., Redondas, A., Hase, F., Guirado, C., Blumenstock, T., and Cuevas, E.: Comparison of ground-based Brewer and FTIR total column O₃ monitoring techniques, *Atmos. Chem. Phys.*, 8, 5535–5550, 2008,

<http://www.atmos-chem-phys.net/8/5535/2008/>. 1226, 1233

Schneider, M. and Hase, F.: Improving spectroscopic line parameters by means of atmospheric spectra: Theory and example for water vapour and solar absorption spectra, *J. Quant. Spectrosc. Ra.*, doi:10.1016/j.jqsrt.2009.04.011, accepted, 2009. 1223, 1226, 1231, 1234, 1242

Spencer, R. W. and Braswell, W. D.: How Dry is the Tropical Free Troposphere? Implications for Global Warming Theory, *B. Am. Meteorol. Soc.*, 78, 1097–1106, 1997. 1222

Vigouroux, C., De Mazière, M., Demoulin, P., Servais, C., Hase, F., Blumenstock, T., Kramer, I., Schneider, M., Mellqvist, J., Strandberg, A., Velazco, V., Notholt, J., Sussmann, R., Stremme, W., Rockmann, A., Gardiner, T., Coleman, M., and Woods, P.: Evaluation of tropospheric and stratospheric ozone trends over Western Europe from ground-based FTIR network observations, *Atmos. Chem. Phys.*, 8, 6865–6886, 2008,

<http://www.atmos-chem-phys.net/8/6865/2008/>. 1223

Vömel, H., Selkirk, H., Miloshevich, L., Valverde, J., Valdés, J., Kyrö, E., Kivi, R., Stolz, W., Peng, G., and Diaz, J. A.: Radiation dry bias of the Vaisala RS92 humidity sensor, *J. Atmos.*

Ocean. Tech., 24, 953–963, 2007. 1227, 1233

Worden, J. R., Bowman, K., Noone, D., Beer, R., Clough, S., Eldering, A., Fisher, B., Goldman, A., Gunson, M., Herman, R., Kulawik, S. S., Lampel, M., Luo, M., Osterman, G., Rinsland, C., Rodgers, C., Sander, S., Shephard, M., and Worden, H.: TES observations of the tropospheric HDO/H₂O ratio: retrieval approach and characterization, J. Geophys. Res., 111(D16), D16309, doi:10.1029/2005JD006606, 2006a. 1226, 1230

Worden, J. R., Noone, D., Bowman, K., Beer, R., Eldering, A., Fisher, B., Gunson, M., Goldman, A., Herman, R., Kulawik, S. S., Lampel, M., Osterman, G., Rinsland, C., Rodgers, C., Sander, S., Shephard, M., Webster, C. R., and Worden, H.: Importance of rain evaporation and continental convection in the tropical water cycle, Nature, 445, 528–532, doi:10.1038/nature05508, 2006b. 1230

Yoshimura, K., Kanamitsu, M., Noone, D., and Oki, T.: Historical isotope simulation using Reanalysis atmospheric data, J. Geophys. Res., 113, D19108, doi:10.1029/2008JD010074, 2008. 1230

AMTD

2, 1221–1246, 2009

**Reviewing
ground-based FTIR
water vapour
analysis**

M. Schneider and F. Hase

Title Page

Abstract

Introduction

Conclusions

References

Tables

Figures

◀

▶

◀

▶

Back

Close

Full Screen / Esc

Printer-friendly Version

Interactive Discussion

Reviewing ground-based FTIR water vapour analysis

M. Schneider and F. Hase

Table 1. Scatter between PWVs of FTIR, RS92 and Cimel sunphotometer for the different FTIR inversion setups. First column: scatter of FTIR–RS92; second column: scatter of FTIR–Cimel sunphotometer; third column: root-square-sum of scatter FTIR–RS92 and FTIR–Cimel. The Cimel data are courtesy of P. Goloub, University of Lille, France (PI of Izaña’s Cimel experiment).

	FTIR –RS92	FTIR –Cimel	RSS
lin	±14.5%	±13.5%	±19.8%
log	±14.1%	±13.4%	±19.5%
log, isc	±13.8%	±13.3%	±19.2%
log, isc, nV	±14.2%	±13.4%	±19.6%
log, isc, nV, ae	±14.2%	±13.3%	±19.5%
log, isc, nV, ae, T	±14.1%	±13.1%	±19.2%

Title Page

Abstract

Introduction

Conclusions

References

Tables

Figures

⏪

⏩

◀

▶

Back

Close

Full Screen / Esc

Printer-friendly Version

Interactive Discussion

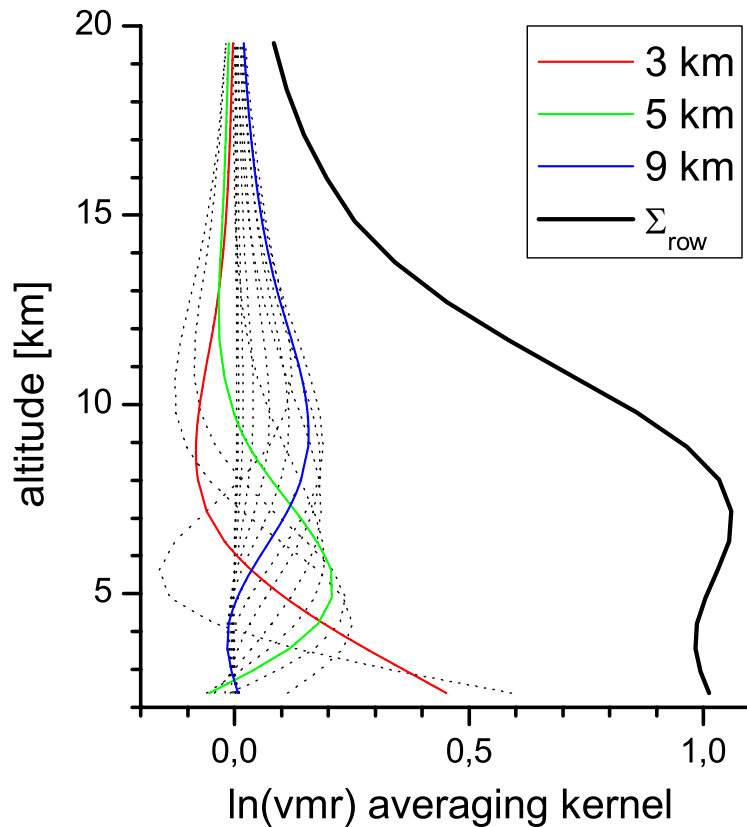


Fig. 1. Typical averaging kernels for ground-based FTIR remote sensing of water vapour. The kernels for 3, 5, and 9 km are highlighted by red, green, and blue colors, respectively. The total sensitivity (Σ_{row}) is depicted as thick black line.

Reviewing
ground-based FTIR
water vapour
analysis

M. Schneider and F. Hase

Title Page

Abstract

Introduction

Conclusions

References

Tables

Figures

◀

▶

◀

▶

Back

Close

Full Screen / Esc

Printer-friendly Version

Interactive Discussion

**Reviewing
ground-based FTIR
water vapour
analysis**

M. Schneider and F. Hase

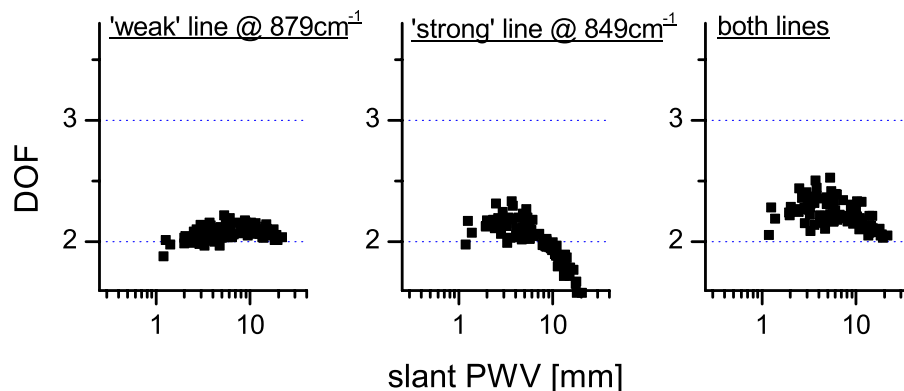


Fig. 2. Dependence of DOF values on slant PWV for the application of different water vapour signatures. Left panel: weak line at 879 cm^{-1} ; middle panel: strong line at 849 cm^{-1} ; right panel: both weak and strong line at 879 cm^{-1} and 849 cm^{-1} .

[Title Page](#)[Abstract](#)[Introduction](#)[Conclusions](#)[References](#)[Tables](#)[Figures](#)[◀](#)[▶](#)[◀](#)[▶](#)[Back](#)[Close](#)[Full Screen / Esc](#)[Printer-friendly Version](#)[Interactive Discussion](#)

Reviewing ground-based FTIR water vapour analysis

M. Schneider and F. Hase

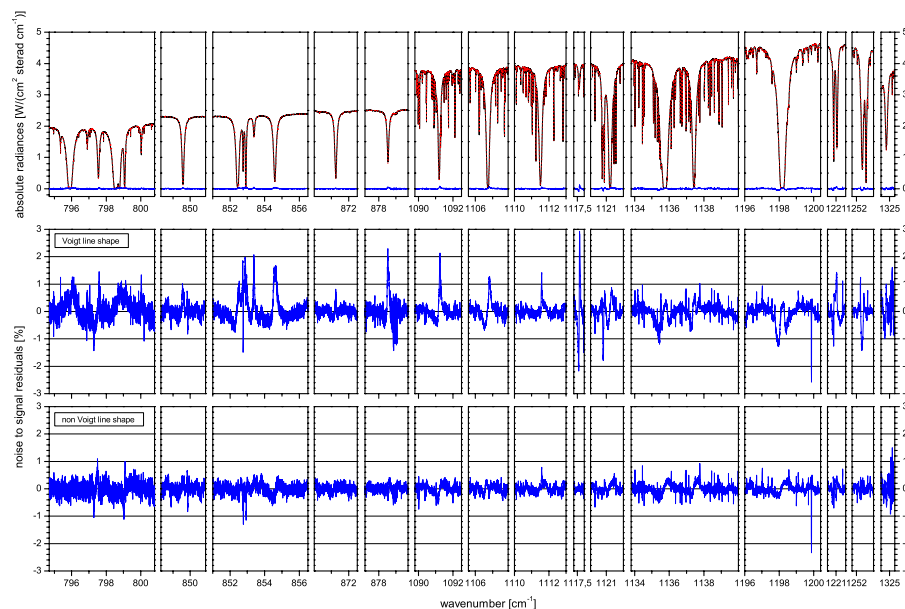


Fig. 3. The 15 spectral windows used for the retrieval of water vapour profiles for typical atmospheric conditions at CIAI (slant PWV of 6.1 mm). The spectral resolution of a typical measurement is 0.005 cm^{-1} . Top panels: black line: measurement; dotted red line: simulation; blue line: residuals (measurement-simulation). Central panels: zoomed out residuals when applying a Voigt line shape model and the HITRAN 2004 parameters (Rothman et al., 2005) with the water vapour update of Gordon et al. (2007) (depicted as noise to signal ratio); bottom panels: same as central panel but for a speed dependent Voigt line shape model and the parameters of Schneider and Hase (2009).

[Title Page](#)[Abstract](#)[Introduction](#)[Conclusions](#)[References](#)[Tables](#)[Figures](#)[⏪](#)[⏩](#)[◀](#)[▶](#)[Back](#)[Close](#)[Full Screen / Esc](#)[Printer-friendly Version](#)[Interactive Discussion](#)

Reviewing ground-based FTIR water vapour analysis

M. Schneider and F. Hase

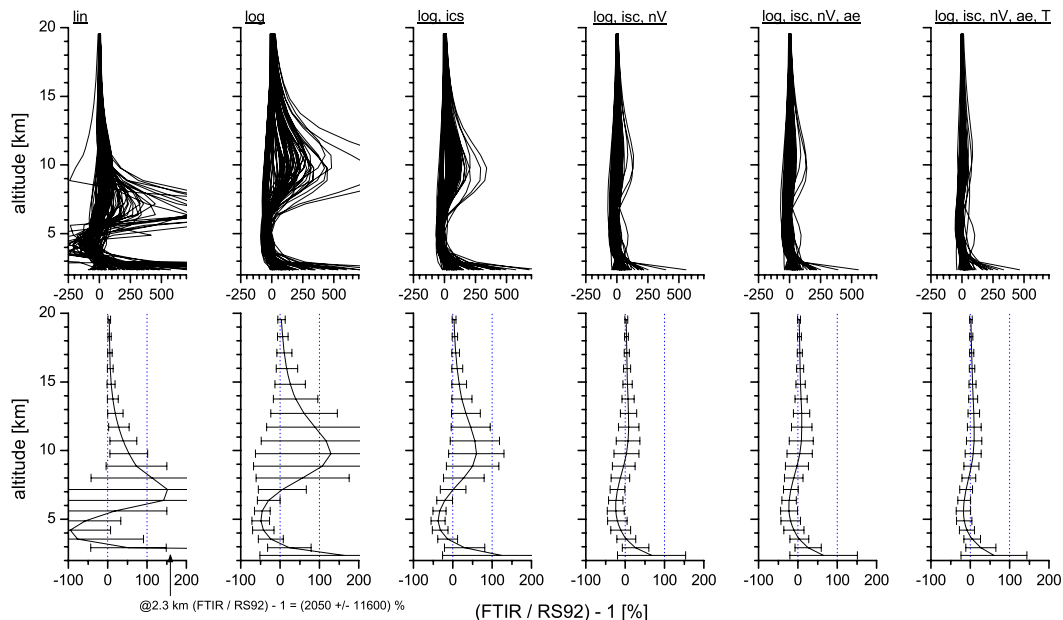


Fig. 4. Difference between smoothed Vaisala RS92 profiles and FTIR profiles for different inversion approaches. Top panels: individual differences for 93 coincidences (between June 2005 and February 2007); bottom panels: statistics of the differences (mean and standard deviation). From the left to the right: lin: inversion on a linear scale; log: inversion on a logarithmic scale; log, isc: log-scale inversion and application of an HDO/H₂O inter-species constraint; log, isc, nV: log-scale, inter-species constraint, and application of a speed dependent Voigt line shape model; log, isc, nV, ae: log-scale, inter-species constraint, speed dependent Voigt line shape, and consideration of atmospheric emission; log, isc, nV, ae, T: log-scale, inter-species constraint, speed dependent Voigt line shape, atmospheric emission, and simultaneous temperature profile inversion.

[Title Page](#)
[Abstract](#)
[Introduction](#)
[Conclusions](#)
[References](#)
[Tables](#)
[Figures](#)
[◀](#)
[▶](#)
[◀](#)
[▶](#)
[Back](#)
[Close](#)
[Full Screen / Esc](#)
[Printer-friendly Version](#)
[Interactive Discussion](#)

Reviewing ground-based FTIR water vapour analysis

M. Schneider and F. Hase

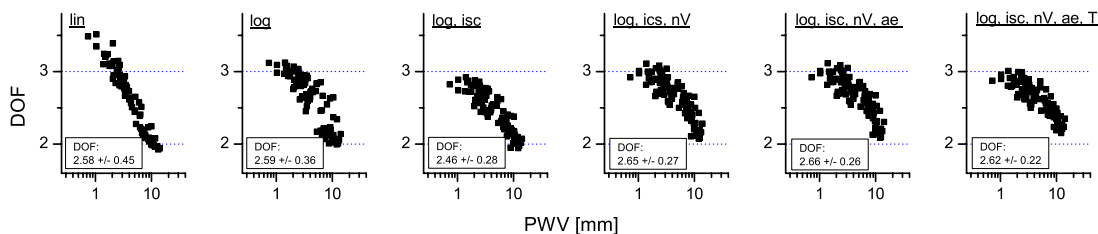


Fig. 5. Dependence of DOF values on PWV for the same different inversion approaches as in Fig. 4. The mean DOF value as well as its 1σ variability are noted in each panel.

Title Page

Abstract

Introduction

Conclusions

References

Tables

Figures

⏪

⏩

◀

▶

Back

Close

Full Screen / Esc

Printer-friendly Version

Interactive Discussion

Reviewing ground-based FTIR water vapour analysis

M. Schneider and F. Hase

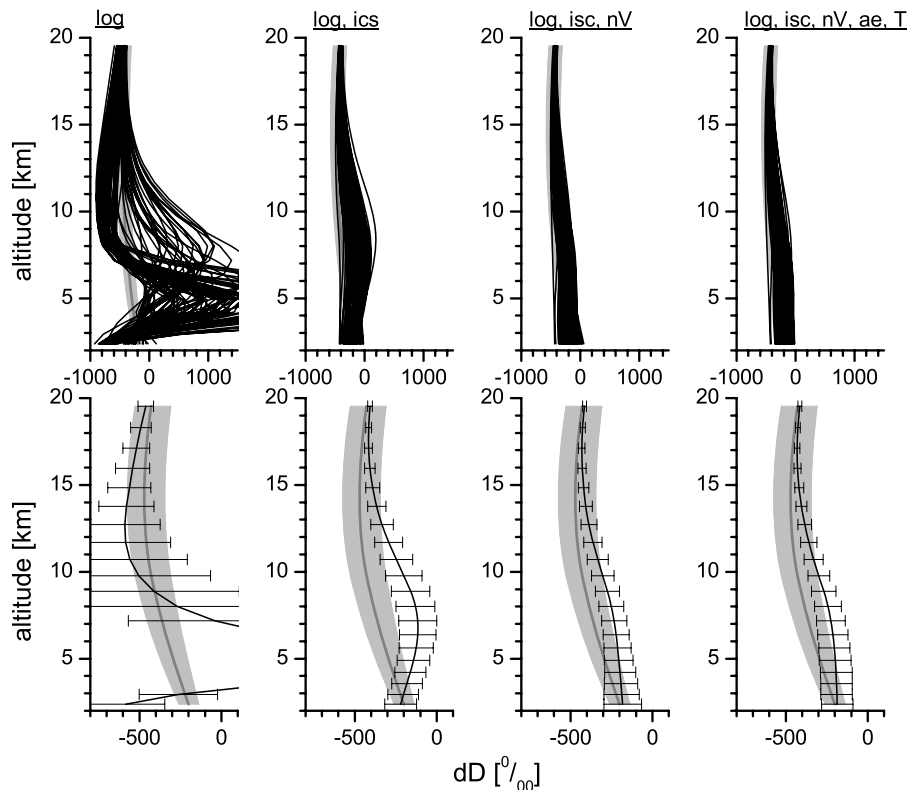


Fig. 6. δD profiles produced by different inversion approaches. Top panels: individual profiles for the ensemble of the FTIR/RS92 coincidences; bottom panels: statistics of the δD profiles (mean and standard deviation). From the left to the right: log: log-scale inversion; log, isc: log-scale inversion and application of an HDO/H₂O inter-species constraint; log, isc, nV: log-scale, inter-species constraint, and application of a speed dependent Voigt line shape model; log, isc, nV, ae, T: log-scale, inter-species constraint, speed dependent Voigt line shape, atmospheric emission, and simultaneous temperature profile inversion.

[Title Page](#)
[Abstract](#)
[Introduction](#)
[Conclusions](#)
[References](#)
[Tables](#)
[Figures](#)
[◀](#)
[▶](#)
[◀](#)
[▶](#)
[Back](#)
[Close](#)
[Full Screen / Esc](#)
[Printer-friendly Version](#)
[Interactive Discussion](#)

Reviewing
ground-based FTIR
water vapour
analysis

M. Schneider and F. Hase

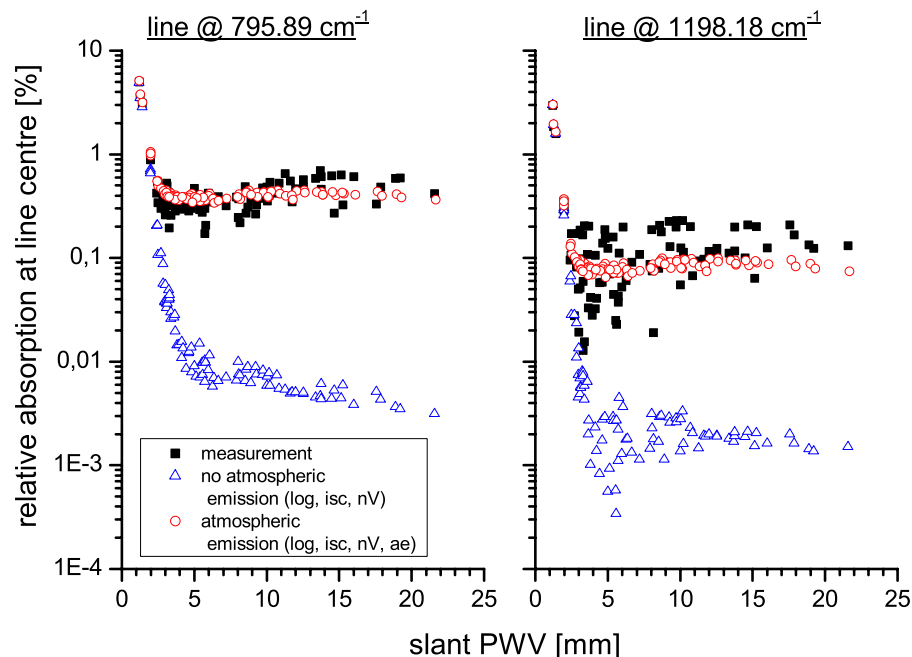


Fig. 7. Relative baseline offset ($\frac{\text{intensity at line centre}}{\text{intensity at line shoulder}}$) at the centres of strong water vapour lines. Left panel: line at low frequency (795 cm⁻¹); right panel: line at higher frequency (1198 cm⁻¹). Black squares: measurement; blue triangle: no consideration of atmospheric emission; red circles: consideration of atmospheric emission.

[Title Page](#)[Abstract](#)[Introduction](#)[Conclusions](#)[References](#)[Tables](#)[Figures](#)[◀](#)[▶](#)[◀](#)[▶](#)[Back](#)[Close](#)[Full Screen / Esc](#)[Printer-friendly Version](#)[Interactive Discussion](#)